What Are the Origins of Stress Relaxation Behaviors in Step Shear of Entangled Polymer Solutions?

Sham Ravindranath and Shi-Qing Wang*

Department of Polymer Science and Maurice Morton Institute of Polymer Science, University of Akron, Akron, Ohio 44325-3909

Received July 6, 2007; Revised Manuscript Received August 14, 2007

ABSTRACT: We apply a recently developed particle-tracking velocimetric (PTV) method along with conventional rheometric measurements to elucidate the nature of one class of nonlinear behavior of entangled polymer solutions under shear. At a fixed degree of chain entanglement, i.e., with the same parent polymer at 10 wt % concentration, we use different liquid media as the solvent to control the upper bound of interfacial wall slip. Contrary to the common perception that these solutions would undergo quiescent relaxation after experiencing a sudden shear strain, we observe macroscopic motions either in the sample interior or at the sample/wall interfaces, corresponding to type A or C behavior, respectively. These macroscopic motions cause the residual stress to decline faster than relaxation due to quiescent molecular diffusion. We illustrate that a continuous range of relaxation behavior can be observed for solutions of the same level of chain entanglement, with one thing in common that the sufficiently strained polymers (with entanglements per chain higher than 10) do not relax the residual stress quiescently upon shear cessation and yield either at the interfaces or in the sample interior due to the retraction force built by the external strain.

1. Introduction

Long flexible linear polymers coil up in a mutually interpenetrating manner leading to chain entanglement. The entanglement interactions have been represented as junctions in a temporary network.[1] The simplest way to probe the effect of chain entanglement and to learn about its strength is to carry out step shear of different strain amplitudes, where a given strain γ is suddenly applied and maintained subsequently. Presumably, how the shear stress relaxes after the step shear reveals the response of the entanglement network to external deformation.

The most serious attempt to offer a theoretical depiction of entangled polymers under external deformation is that of the Doi−Edwards tube theory.[2] In this theory, a test chain is placed in a tube to depict the entanglement constraints imposed by surrounding chains, and an instantaneous step shear produces affine deformation of the test chain. Upon shear cessation, the deformed test chain was perceived to retract within the tube on a time scale of Rouse time τ_R, leading to a kinklike characteristic drop of the predicted shear stress.[2] The remaining shear stress would relax through reptation[3] of the test chain out of the tube. Hence, at large step strains, the DE theory anticipate an entangled polymer to exhibit two-step relaxation dynamics. The entanglement network is perceived to remain intact both during and after shear. It is the perceived quiescent chain relaxation dynamics and diffusion within the constraints of entanglement that was thought to dictate the observed stress decay in any previous theoretical treatment including the DE theory. For quiescently relaxing systems, it is legitimate to characterize stress relaxation with material functions such as a strain-dependent relaxation modulus $G(t,\gamma) = \sigma(t)/\gamma$, where the magnitude of the resulting shear stress σ is normalized with the amplitude γ of the applied step shear. The DE theory found it more convenient to evaluate a damping function $h(\gamma)$ defined as

$$h(\gamma) = G(t,\gamma)/G_e(t), \quad \text{for } t > \tau_R \tag{1}$$

where the equilibrium relaxation modulus $G_e(t)$ is the relaxation modulus $G(t,\gamma)$ obtained for $\gamma \ll 1$. Since the long-time shear stress $\sigma(t)$ was predicted to have the same time dependence regardless of γ, h is introduced to show only the strain dependence of the relaxation characteristics. Any drop of h with γ would reflect strain softening of the entanglement network.

Initial experimental reports of step shear deformation dated back to the early 1970s.[4−6] Since the advent of Doi−Edwards tube theory,[7,8] it has been routine to present the shear stress relaxation data in terms of the damping function h. Most experiments are based on either polystyrene[9−14]or polybutadiene[15−17] solutions. Summarizing all the rheological observations of step shear over the past 3−4 decades, it can be said that nearly half of the studies[18,19] found reasonable agreement[10] with the Doi−Edwards theoretical prediction for h and were therefore regarded as *normal*. On the other hand, samples with sufficiently high entanglement density typically showed excessive strain softening[9,20] when compared to the DE damping function h, while some experimental data actually displayed a damping function well above the DE prediction.[15] In the literature, these three types of experimental results have been classified as normal type A and kinklike type C and type B behavior, respectively,[18] where type B behavior usually involved weakly entangled solutions.

Well-entangled polymer solutions usually produce type C behavior. For PS solutions, there has appeared an empirical criterion involving the product of concentration ϕ and molecular weight M. Paradoxically, these strongly entangled systems have weaker finite-size effects and should supposedly fit the tube model description better. To account for the type C behavior, a free energy argument was put forward to indicate the possibility of strain inhomogeneity in a largely deformed sample upon shear cessation.[21] This idea of inhomogeneous strain was further elaborated in a subsequent study within the framework of the DE theory.[11] No specific molecular mechanism was put forward concerning the origin of such inhomogeneous deformation. Subsequently, on the basis of crude particle tracking observations, a delayed slip phenomenon was reported after shear cessation in a solution that showed type C behavior.[12] In many

* Corresponding author: e-mail swang@uakron.edu.

10.1021/ma071495g CCC: $37.00
Published on Web 09/29/2007

Table 1. Molecular Characteristics of Long Chain PBDs

sample	M_n (g/mol)	M_w (g/mol)	M_w/M_n	source
1M	1.014×10^6	1.052×10^6	1.03	University of Akron
0.7M	0.74×10^6	0.75×10^6	1.02	Bridgestone

studies of type C behavior, failure of the Lodge−Meissner relation was also reported.[13]

More recently, Archer and co-workers have shown that the same solution could shift from type C to type A behavior depending on the surface condition of the cone−plate fixture.[14,16] Using short PBD chains as solvent, the same group also reported[17] a transition from type A to type C with increasing level of entanglements per chain ($Z > 54$). These observations have reinforced the speculation[18,19] that type C behavior is perhaps an experimental artifact, in part related to slip.

In 2006, through reexamination of the original DE theoretical prediction and revelation by particle tracking velocimetry (PTV) of nonquiescent relaxation after step strain, Wang et al.[22] showed that the normal type A behavior was anything but normal. The observed macroscopic motions appear to indicate breakup of the entanglement network, leading to the "normal" strain softening that coincides with the DE theoretical description. This set of PTV observations of step shear has allowed a first peek into how chain entanglements may dissolve due to buildup of sufficient retractive forces and thus offered crucial insight into relevant ingredients[23] that must be taken into account in any theoretical description of polymer entanglements during and after external deformation.

In this work, we show that there is always macroscopic motion upon a step shear beyond certain strain amplitude, either due to internal structural breakup or interfacial wall slip. Because of occurrence of nonquiescent relaxation, no material functions such as the relaxation modulus can be meaningfully defined. Thus, the classification of type A, B, or C relaxation behavior is essentially arbitrary. In this paper, we show that a full range of type A to C behavior can take place for PBD solutions of same entanglement level ($Z = 40$) that possess different abilities to undergo interfacial wall slip.

2. Experimental Section

2.1. Materials. Entangled 1,4-polybutadiene (PBD) solutions were prepared by first dissolving a desired wt % of high molecular weight PBD in toluene. To this solution either ditridecyl phthalate (DTDP) or low molecular weight oligomeric PBDs was added and mixed. Silver-coated particles with an average diameter of 10 μm (Dantec Dynamics HGS-10) were first ultrasonicated in toluene and then added to the mixture. The final loading of the particles was at a level of 200−600 ppm. Toluene was allowed to evaporate at room temperature for nearly a week under hood. Residual toluene was completely removed under vacuum for about 48 h. 1M(10%)-15K sample refers to 10 wt % of the sample 1M (listed in Table 1) dissolved in 90 wt % of 15K oligomeric PBD (listed in Table 2). Similarly, the other three solutions are labeled as 1M(10%)-1.8K, 1.0M(10%)-DTDP, and 700K(5%)-DTDP. The molecular characteristics of the high molecular weight PBDs and the solvents are given in Table 1 and Table 2, respectively. The properties of the entangled solutions are shown in Table 3.

2.2. Apparatuses. Step shear experiments were carried out on a stress-controlled Bohlin-CVOR rheometer at room temperature. Cone−plate disks of 25 mm diameter and cone angle of 5.4° were employed in all of the measurements. Advanced Rheometrics Expansion System (ARES) was used for small-amplitude oscillatory shear (SAOS) frequency sweep measurements at room temperature.

2.3. Particle Tracking Velocimetry (PTV) Setup. Silver particles embedded in the sample are illuminated by passing a laser sheet with a cross section of 0.2 mm × 2 mm across the gap at an angle, as shown in Figure 1. The movement of the illuminated particles across the entire sample thickness is captured with a black−white CCD camera (with a maximum speed of 30 frames/s) and recorded on a videotape. The CCD camera is mounted with a DIN objective lens (3.2×) through an adaptive tube (Edmund Optics: U54-868). During analysis, the distance traveled by a particle can be determined by playing 1−3 frames using MGI Videowave 4 software. PTV observations were typically made at a radial distance of 4.5 mm from the edge. The spatial resolution of our PTV is around 30 μm since the tracking particle size range from 10 to 20 μm.

3. Theoretical Background

The apparent agreement[10] of the experimental type A behavior with Doi−Edwards tube theory has been taken as a great success of the theory.[2] On the other hand, the confusion produced by the type C behavior is related to a lack of clear theoretical understanding of how entangled polymers may undergo interfacial wall slip.

A. Wall Slip Due to Lack of Entanglement at Sample/Wall Interface. Slip boundary condition depicts polymer flow in presence of containing walls when entanglement interactions are lost at the polymer/wall interface through either chain desorption or disentanglement. Lack of interfacial chain entanglement leads to a great disparity between the bulk viscosity η and the interfacial viscosity η_i. The most effective way to describe the consequence of a huge ratio of η/η_i is to introduce the Navier−de Gennes extrapolation length b, as shown in Figure 2 and given below[24]

$$b = (\eta/\eta_i)a \tag{2}$$

where the thickness a of the entanglement-free interfacial layer is a molecular scale perhaps comparable to the entanglement spacing l_{ent}. For solutions, η_i can be as low as the solvent viscosity η_s, and the entanglement spacing l_{ent} would grow upon dilution according to

$$l_{ent}(\phi) = l_{ent}(\phi=1)\phi^{-2/3} \tag{3}$$

that has been established both theoretically[25] and experimentally[26,27] where ϕ is the polymer weight or volume fraction. The modification of a simple shear due to slip is measured in terms of b/H, as illustrated in Figure 2.

Wall slip is a leading form of inhomogeneous shear in polymer flow. Interestingly, unlike the case of melts, the magnitude of wall slip for solutions can be effectively altered by selecting different values for η_i in eq 2. Most of the previous step shear experiments employed a small molecule liquid as the solvent for entangled solutions. As a consequence, a great amount of wall slip is possible upon a step shear as observed previously[12,28] because of the exceedingly low value of $\eta_i \sim \eta_s$. In other words, a solution does not need to be as entangled as a melt to suffer more wall slip when a solvent of water-like viscosity is used to prepare the solution.

B. Magnitude of Interfacial Slip. Conversely, the effect of wall slip can also be greatly minimized for solutions by using an entangled polymeric solvent of molecular weight M_1 with the same chemical structure as the "parent" polymer of molecular weight M so that the viscosity ratio upon interfacial chain disentanglement is

$$\eta/\eta_i = (M/M_1)^{3.4} \tag{4}$$

which can be a significantly reduced number from $\eta/\eta_e = (M/M_e)^{3.4}$ in the case of slip of melts provided that $M_1 > M_e$. To estimate b, we take the interfacial thickness to be l_{ent} of eq 3

Table 2. Molecular Characteristics of Various Solvents

sample	M_n (g/mol)	M_w (g/mol)	M_w/M_n	source	η_s (Pa s)
PBD-15K	14020	15000	1.07	Bridgestone	36
PBD-1.8K	1800			Sigma-Aldrich Cat. No. 20,043-3	97
oil (DTDP)	530	530	1	Imperial oil	0.2

Table 3. Properties of PBD Solutions

solution	M_w/M_e	τ (s)	τ_R (s)	η (Pa.s)	η/η_s	l_{ent} (nm)	b (mm)
1M(10%)-DTDP	40	18.3	0.45	60484	302420	17	5.1
1M(10%)-15K	40	66.6	1.66	2.5×10^5	6944	17	0.12
1M(10%)-1.8K	40	285.7	7.14	1.25×10^6	12886	17	0.22
0.7M(5%)-DTDP	13	1.25	0.096	773	3865	27	0.10

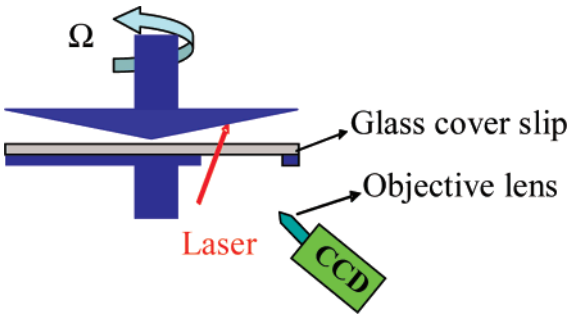

Figure 1. Schematic drawing of our particle-tracking velocimetric apparatus.

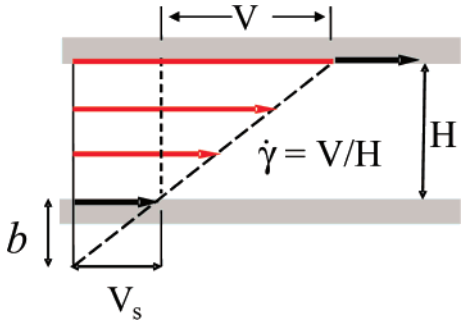

Figure 2. Depiction of wall slip where the slip length b characterizes the effect of interfacial slip on shear deformation of a sample of thickness H in terms of the slip velocity V_s and shear rate V/H. Here the importance of slip is naturally measured by $b/H = V_s/V$.

and find, with l_{ent} ($\phi = 1$) = 3.8 nm for 1,4-PBD, l_{ent} to be ca. either 17 nm at 10 wt % or 27 nm at 5 wt %, as listed in Table 3. On the basis of the viscosity ratios calculated from the small-amplitude oscillatory shear measurements in Figures 3a, 4a, 5a, and 6a, the values of b are estimated in Table 3, ranging from a huge magnitude of 5 mm to a negligible number of 0.12 mm, as the viscosity ratio gets suppressed by a factor of 43, with the solvent changed from a hydrocarbon oil to PBD of M_w = 15 kg/mol for the two 10% PBD solutions made from the same parent PBD of $M_w = 1.052 \times 10^6$.

C. Cohesive Failure in Solutions Based on Polymeric Solvents. In deformations that either take place very slowly (i.e., on a time scale longer than the terminal relaxation time τ) or are small in amplitude (i.e., the shear strain $\gamma \ll 1$), chain entanglement pervades all the way from the bulk (i.e., interior) to the boundaries that contain the sample. In other words, chains adsorbed at the surfaces could remain entangled with the unbound bulk chains through mutual penetration. In the case of melts or solutions based on binary mixtures such as 1M-(10%)-15K, the long chain adsorption can be rather strong at such common surfaces found in rheological apparatuses as steel and aluminum. Upon a large deformation, disentanglement would typically first take place involving the monolayer of adsorbed chains. In the event where the effect of such interfacial slip is made negligible by the choice of a polymeric solvent, infinitesimal interfacial wall slip alone is insufficient to cause rapid relaxation of the residual stress, and the surviving residue stress can force the system to undergo internal network breakup through *bulk* chain disentanglement[23] away from the polymer/wall interface.

As the magnitude of interfacial slip varies with the viscosity ratio, from one sample to another, the nonquiescent relaxation may involve different levels of interfacial and internal breakdown of chain entanglement, giving rise to relaxation behavior from type C to type A. Below we apply PTV to elucidate the different kinds of nonquiescent relaxation and to reveal what really happens in these conventional rheological measurements of the "relaxation modulus" or "damping function" that has previously been used to categorize a range of relaxation behavior from type A to type C.

4. Results and Discussion

With the exception of PBD melts,[29] most experimental studies of stress relaxation after large step strains were based on polystyrene[9−14] and polybutadiene[15−17] solutions. Empirically, these samples were found to exhibit normal type A behavior in agreement with the DE theory when the level of entanglement is not excessively high. Solutions based on small-molecule solvents often exhibit type C behavior at higher levels of entanglement obtained at higher concentrations and/or with higher molecular weights of the parent polymer. In this paper, we adopt PBD solutions as model systems to illustrate the physics behind the various types of relaxation behavior. Although speculations have been abundant concerning the origins of relaxation behavior from type A to C,[18,19] it remains to be shown in this work how interfacial slip and/or bulk failure of the entanglement network produce a continuous spectrum of relaxation behavior after large step strains, from type A to C.

A. Equally Entangled Solutions Showing Type A/B and Type C Behavior. Below we present results from three solutions at the same concentration and thus identical level of entanglement. These solutions are made of 10 wt % 1,4-polybutadiene (1M) as shown in Table 1 in three different solvents of 1,4-PBD of M_w = 15 kg/mol, 60% unsaturated PBD of high vinyl content with M_w = 1800 g/mol, and a hydrocarbon oil (DTDP). As indicated in Table 3, their ability to undergo wall slip varies greatly. We will begin with 1M(10%)-15K, which has been designed to undergo negligible interfacial slip.

1. Type B/A Behavior in 1M(10%)-15K. Small-amplitude oscillatory shear frequency sweep was first carried out to determine the basic linear viscoelastic characteristics, as shown in Figure 3a. A high shear rate $\dot{\gamma}$ corresponding to Weissenberg number $\tau\,\dot{\gamma} = 930$ was applied for different durations in each discrete step shear experiment to produce strain amplitudes γ ranging from 0.1 to 8.4, as shown in Figure 3b. Even though

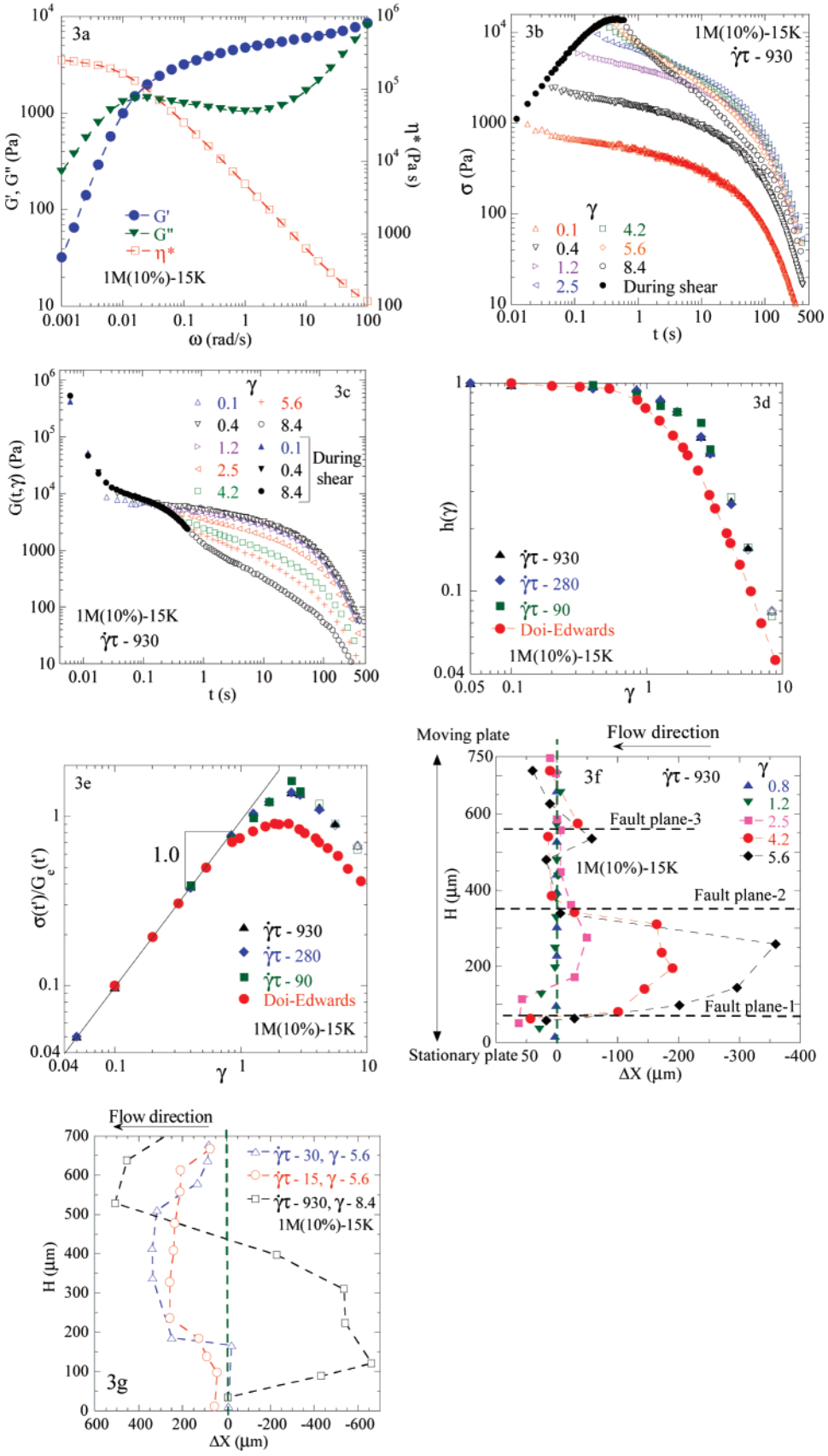

Figure 3. (a) Small-amplitude oscillatory shear measurements of storage, loss moduli (G', G''), and the complex viscosity $|\eta^*|$ as a function of frequency. (b) Shear stress growth and relaxation during and after discrete step shearing of different magnitudes, where the Weissenberg number $\dot{\gamma}\tau$ is 930. (c) Relaxation modulus evaluated from (b) to normalize the data with the strain magnitude γ. (d) Damping function h that represents the relaxation conditions at long times from different tests involving different applied shear rates. The open symbols designate step strains where a stress overshoot emerges during shear. (e) Direct measure, $\gamma h(\gamma)$, of the stress relaxation by normalizing the data in (b) at long times with the equilibrium relaxation modulus, G_e, shows a nonmonotonic relationship with γ. (f) Particle-tracking velocimetric (PTV) detection of macroscopic motions after various discrete step strains where the final positions of the tracked particles are given. (g) PTV description of the macroscopic motions upon shear cessation beyond stress overshoot.

the stress relaxation does not reveal a kinklike sharp drop except for $\gamma = 8.4$ that produced a stress overshoot, the relaxing stress level in the superimposable region is actually lower for $\gamma = 4.2$ than for $\gamma = 2.5$. Similarly, in the superimposable region, the relaxing stress level is lower for $\gamma = 5.6$ than for $\gamma = 1.2$. This behavior is observed in spite of buildup of significantly higher stress with increasing γ, as indicated by the filled circles in Figure 3b, and did not catch attention in the literature because the conventional representation of the stress data in Figure 3b is to plot the "relaxation modulus" according to $G(t) = \sigma(t)/\gamma(t)$, as shown in Figure 3c, where the initial values of $G(t)$ are included at times before the completion of the step strain.

Traditionally, one chooses to simplify the representation in terms of the damping function h of eq 1, recognizing that the stress decay is eventually the same at long times, i.e., in the superimposable region, as evident from the experimental data in Figure 3b,c. Figure 3d summarizes our rheological measurements in terms of the damping function, along with the Doi−Edwards (DE) theoretical prediction (in filled circles), where the different symbols denote results obtained using different shear rates. The relaxation behavior would be labeled type B because it shows considerably weaker strain softening than the DE prediction. Unfortunately, this representation of the relaxation behavior in term of h of eq 1 disguised a hidden character shared by both such step strain experiment and DE theory, as shown Figure 3e: the partially relaxed stress levels in the superimposable region are actually lower for higher values of the imposed γ. Such a nonmonotonic feature of the DE theoretical prediction has gone unnoticed until recently.[22] More importantly, the experimental data reveal the same unexpected nonmonotonicity. To our judgment, this is possible only if the entanglement network has suffered breakup because an intact network should always resist with a higher shear stress to a higher imposed γ. We have recently offered a theoretical account of the yielding criterion and explained why entanglement network is so fragile and easy to break down due to large external deformation.[23]

In passing, we note that in Figure 3d,e the open symbols designate those step strain experiments where shear stress overshoot emerged before reaching the prescribed strain amplitude. For example, at the Weissenberg number of 930, the stress overshoot occurred before $\gamma = 8.4$, as shown in Figure 3b. Our previous PTV observations have revealed emergence of inhomogeneous shear beyond the overshoot.[30,31] Therefore, these results have produced insight into why kinklike stress decline can occur at high enough strains: stress relaxation can be speeded up in presence of a preexisting inhomogeneous strain field, and kinklike behavior is more likely to take place for step strains exceeding the point of stress overshoot.

The nonmonotonicity in Figure 3e motivates us to carry out in-situ particle tracking velocimetric (PTV) observations and find out why the sample at higher imposed strains displayed lower relaxed stresses. Figure 3f depicts the nonquiescence in terms of where some of the tracked particles moved after the shear cessation. Our PTV measurements also confirm that there is indeed *quiescent* relaxation for imposed strains as low as 120%, at and below which it would be meaningful to characterize stress relaxation dynamics with relaxation modulus or damping function. Moreover, the experimental data clearly stay above the DE theoretical prediction in Figure 3e for γ at and below 1.2 where the comparison between experiment and theory should be meaningful in absence of any observable macroscopic motion. This discrepancy originates from the fact that the DE theory allows full chain retraction to occur even for $\gamma < 1.0$. In reality and a new theoretical consideration,[23] chain retraction of the kind anticipated by the DE theory does not and cannot occur below a critical strain amplitude[22] of ca. 1.4.

Figure 3f shows that the magnitude of macroscopic motion increases strongly with increasing γ. At $\gamma = 4.2$, there are actually three "fault" planes visible where the tracked particles moved in opposite directions after step shear. The stress relaxation was accelerated because of the internal sample recoil through these fault planes. The speedup of these nonquiescent relaxation relative to the quiescent relaxation below $\gamma = 1.2$ is indeed visible from Figure 3b. At a high strain, the sample may recoil with such a sufficient magnitude that by the time when the macroscopic motion ceases the residual stress could already be lower than a stress level resulting from a low imposed strain. This is how the nonmonotonic behavior is produced in Figure 3e.

Figure 3g shows that the macroscopic motions inside the sample are more intense at the higher strains than those depicted in Figure 3f. Unlike the observations made in Figure 3f where the step strain involved uniform shear, stress overshoot has emerged before shear cessation for the conditions examined in Figure 3g. Thus, upon shear cessation, not only the sample could recoil along the "fault" planes already formed during shear, as shown around $y = 170$ μm for Weissenberg number = 30 in Figure 3g, but there is also residual stress *variation* across the gap that alone could cause macroscopic motions in the sample interior despite the fixed no-slip boundary conditions at the two containing surfaces after shear cessation.

2. Type C Behavior in 1M(10%)-oil. In contrast to the 1M-(10%)-15K, at the same level of chain entanglement, this second solution is capable of massive wall slip upon replacing the slip-suppressing PBD-15K with ditridecyl phthalate (DTDP), a hydrocarbon oil. From the small-amplitude oscillatory shear measurements of its linear viscoelastic properties shown in Figure 4a, we estimate the extrapolation length b of this solution to be around 5 mm, as listed in Table 3.

In the preceding subsection 4.A.1, we observed macroscopic motions only in the sample interior even though the sample/wall interfaces could fail first. It is easy to show how the magnitude of wall slip estimated by the ratio b/H determines whether the sample could take advantage of slip to recoil and relax its residual stress at a rate much faster than that allowed by chain diffusion in quiescence. Given a sample thickness H, any appreciable nonquiescent stress relaxation due to wall slip should arise from macroscopic recoil over a distance Δx comparable to H. The time scale involved in such a recoil via slip is then given by $\Delta t \sim \Delta x/V_s \sim H/(\sigma/\beta)$, where the interfacial friction coefficient is given by[24,32] $\beta = \eta_i/a$. In terms of b of eq 2, we proceed to write $\Delta t \sim (H/b)/(\sigma/\eta) \sim (H/b)(\tau/\gamma)$, where we have $\sigma \sim G\gamma$ and $\eta \sim G\tau$, with γ being the amplitude of the step strain, σ being the stress level at the end of the step shear, and τ being the terminal relaxation time. For $b/H \ll 1$, $\Delta t \gg \tau$: the time taken for the sample to recoil via wall slip is much longer than the relaxation time τ. Thus, for $b/H \ll 1$, interfacial slip cannot accelerate the stress relaxation and plays no role in the preceding solution of 1M(10%)-15K, whose b is no greater than 0.12 mm.

Conversely, with $b/H \gg 1$ in 1M(10%)-oil solution, sample recoil due to interfacial slip can occur on a time scale shorter than the terminal relaxation time τ, thus greatly accelerating the stress relaxation. Figure 4b,c shows the actual stress σ and its normalization, i.e., "relaxation modulus", $G(t) = \sigma(t)/\gamma(t)$, as a function of time. Comparing Figure 4c with Figure 3c, the kinklike stress drop is evident for the 1M(10%)-oil solution at

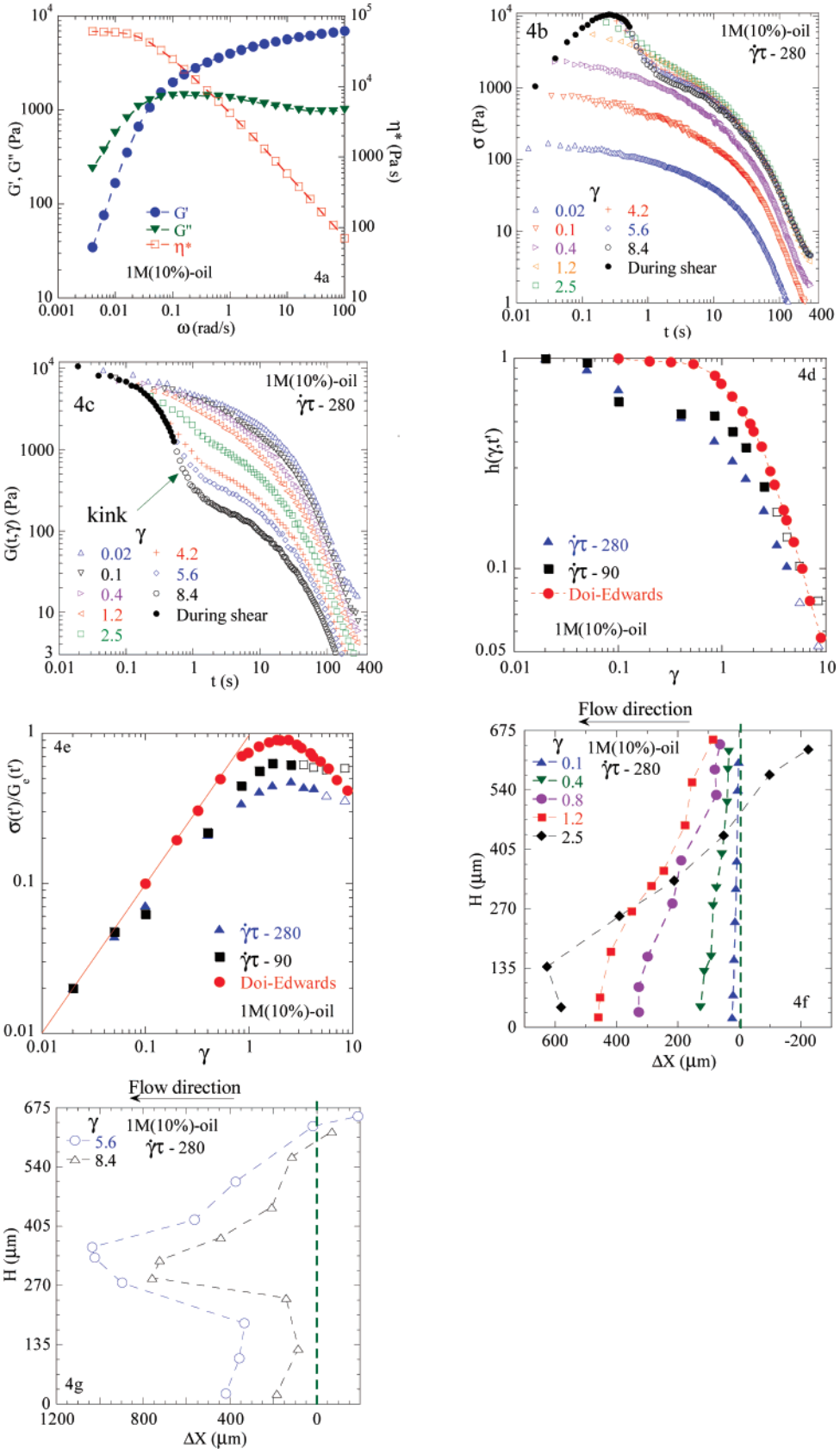

Figure 4. (a) Small-amplitude oscillatory shear measurements of storage, loss moduli (G', G''), and the complex viscosity $|\eta^*|$ as a function of frequency. (b) Shear stress growth and relaxation during and after discrete step shearing of different magnitudes, where the Weissenberg number $\dot{\gamma}\tau$ is 280. (c) Relaxation modulus evaluated from (b) to normalize the data with the strain magnitude. (d) Damping function h that represents the relaxation conditions at long times from different tests involving different applied shear rates. The open symbols designate step strains where a stress overshoot emerges during shear. (e) The normalized stress level given by $\gamma h(\gamma)$ at long times where the stress tends to level off due to interfacial slip, in contrast to Figures 3e, 5b, and 6c. (f) Particle-tracking velocimetric (PTV) detection of macroscopic motions after various discrete step strains where the final positions of the tracked particles are given. (g) PTV description of the macroscopic motions upon shear cessation beyond stress overshoot.

the strains equal to and higher than 2.5, but only visible in the 1M(10%)-15K solution at the highest strain amplitude beyond the stress overshoot.

The conventional "damping function" h in Figure 4d indicates that the sample shows type C behavior. Figure 4e further indicates that even at imposed strains below 1.0 the sample shows lower stresses than the DE prediction and consequently lower than those of the 1M(10%)-15K solution. Since there is neither bulk nor interfacial failure in 1M(10%)-15K below $\gamma = 1.0$, we can tell from such a comparison, even without performing PTV observations, that the 1M(10%)-oil solution must have suffered interfacial slip at these low strains.

Our PTV observations indeed reveal sample recoil due to interfacial wall slip, as shown in Figure 4f. These PTV measurements confirm the key difference between the two solutions: The one based on hydrocarbon oil relieves its residual stress by interfacial slip, a mode of failure that is ineffective in the other solution (1M(10%)-15K) due to the suppression of wall slip by the polymeric solvent PBD-15K. Wall slip is even more severe at higher imposed strains. Indeed, as suggested in the past,[12,18,19] our PTV visualization shows that the type C relaxation behavior can occur readily in entangled polymers that undergo massive slip upon step shear. Finally, we note that this type C behavior amounts to having nearly all data points in Figure 4d below that of the Doi−Edwards curve. Clearly, the DE curve is arbitrary: Independent of whether the data are above or below (i.e., type B and type C) this curve, these samples display *nonquiescent* relaxation and thus cannot be depicted by any theory that is constructed to describe quiescent relaxation.

Figure 4g records macroscopic motions for $\gamma = 5.6$ and 8.4 beyond the point of stress overshoot. Beyond the stress overshoot, the residual stress level is lower at $\gamma = 8.4$ than at 5.6. As consequence, there is actually higher magnitude of macroscopic motions for $\gamma = 5.6$ than for 8.4. Another interesting feature is that maximum movements no longer occur at the interfaces. This is possible only if the state of chain entanglement is no longer uniform across the gap upon shear cessation. In other words, apart from interfacial failure, the interior of the entanglement network must have also suffered breakdown during and after shear.

3. Type A/B Behavior in 1M(10%)-1.8K. The third solution, based on the same parent polymer at 10 wt % concentration, involves a second oligomeric PBD that produces an equally small extrapolation length b as that of the first solution. Since this solvent is of high glass transition temperature and is most sluggish of all, b would be as small as estimated in Table 3 if the interfacial viscosity η_i in eq 2 is indeed dictated by the solvent viscosity η_s. Figure 5a confirms that indeed this solution has the highest zero-shear viscosity due to the high value of η_s. On the other hand, the solution indeed appears to possess a small enough b judging from Figure 5b. In other words, the relaxation characteristics in Figure 5b show strain softening that is only slightly weaker than the ideal type A behavior represented by the DE curve. We recall that the type A data of ref 10 also stay slightly above the DE curve.

Amazingly, our PTV observations indeed support the idea that this solution does not display much interfacial slip. Like the first solution, the sample undergoes macroscopic motions in the sample interior upon step shear, as shown in Figure 5c. Apparently the oligomeric solvent is sufficient to suppress wall slip as an effective mode to relax the residual stress: the sample has to break up internally due to a higher than critical level of residual stress.

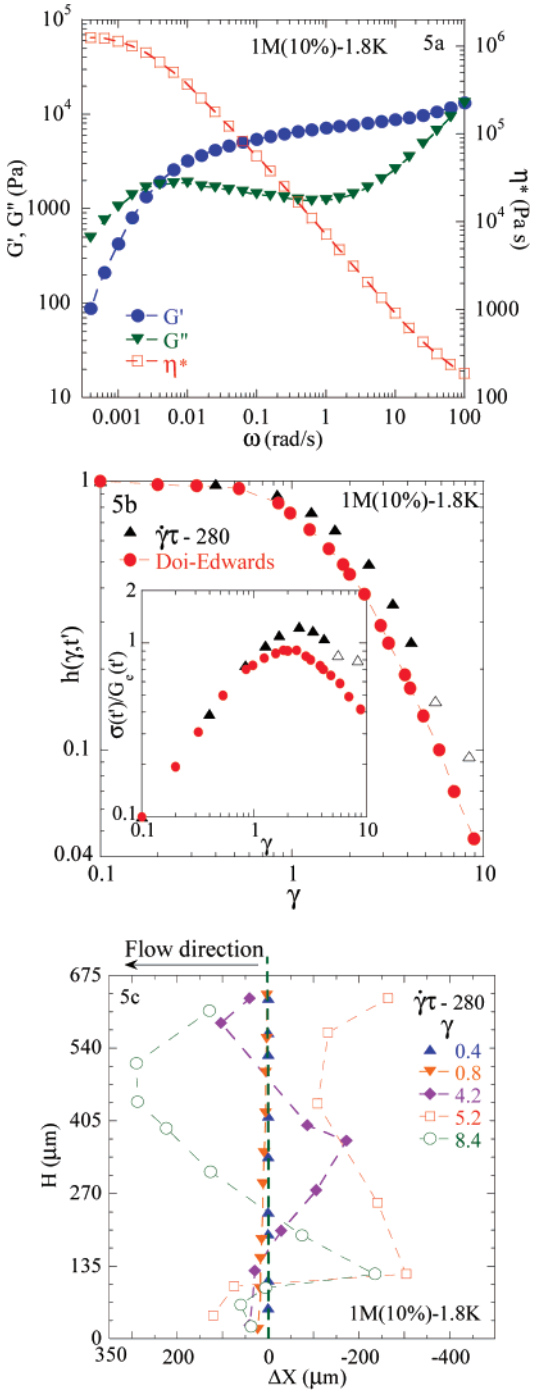

Figure 5. (a) Small-amplitude oscillatory shear measurements of storage, loss moduli (G', G'') and the complex viscosity $|\eta^*|$ as a function of frequency. (b) Damping function h that represents the relaxation conditions at long times from different tests involving different applied shear rates. The open symbols designate step strains where a stress overshoot emerges during shear. The inset shows the normalized stress level given by $\gamma h(\gamma)$ at long times revealing nonmonotonic relationship with γ. (c) Particle-tracking velocimetric (PTV) detection of macroscopic motions after various discrete step strains where the final positions of the tracked particles are given. The open symbols denote the larger step strains beyond stress overshoot.

B. Less Entangled Solution Showing Type A Behavior. We can further explore the characteristics of step shear by studying a solution of a reduced level of entanglement. Specifically, Figure 6a shows the linear viscoelastic properties of the 0.7M(5%)-oil solution where the number of entanglements per chain is reduced from 40 to 13, as shown in Table 2. Comparing the solution viscosities, we see b of 0.7M(5%)-oil

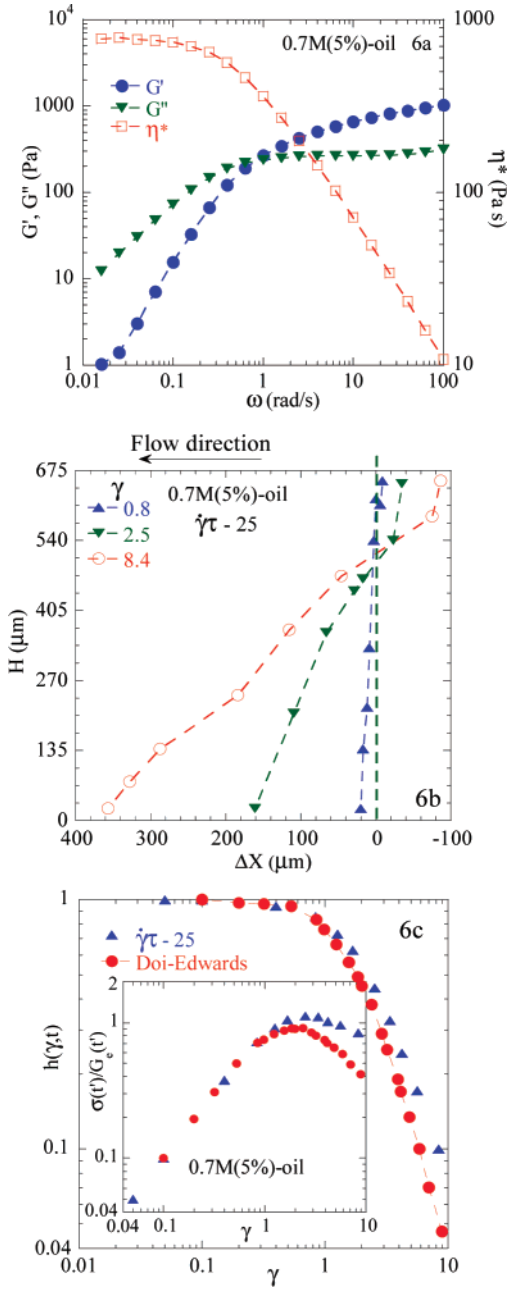

Figure 6. (a) Small-amplitude oscillatory shear measurements of storage, loss moduli (G', G''), and the complex viscosity $|\eta^*|$ as a function of frequency. (b) Particle-tracking velocimetric (PTV) detection of macroscopic motions after various discrete step strains where the final positions of the tracked particles are given. The open circles denote the larger step strains beyond stress overshoot. (c) Damping function h that represents the relaxation conditions at long times from different tests involving different applied shear rates. The open symbols designate step strains where a stress overshoot emerges during shear. The inset shows the normalized stress level given by $\gamma h(\gamma)$ at long times revealing nonmonotonic relationship with γ.

to be smaller than b of 1M(10%)-oil by a factor of 51. Consequently, interfacial slip is expected to produce much less effect on the stress relaxation. With much reduced slip comes significantly less sample recoil and considerably smaller stress decline, as the comparison between Figure 4f and Figure 6b shows.

Several points are worth noting. First, given the small value of b/H, the observed sample recoil shown in Figure 6b cannot be due to the interfacial slip involving only a monolayer because any sample recoil due to slip alone would take a time $\Delta t \gg \tau$ for $b/H \ll 1$ according to our preceding analysis in section 4.A.2. Our PTV technique does not have adequate spatial resolution to determine the layer thickness where the entanglement network breakdown took place. Nevertheless, chain disentanglement must have taken place in a finite layer to produce the observed recoil measured in Figure 6b. Second, even though this solution is also based on DTDP, there is insufficient wall slip to allow type C relaxation behavior. In fact, this 5% solution show relaxation behavior that is closest to the type A behavior, as shown in Figure 6c. This is one more example to show that the classification of the various relaxation behaviors of different entangled polymeric systems into type A to C is entirely arbitrary.

5. Conclusion

Stress relaxation behavior after a step strain is the simplest experiment to probe nonlinear response of an entangled polymer as long as the sudden deformation can take place on time scales much shorter than the terminal relaxation time. Classically, there was the perception that the entanglement network formed of linear polymer chains would be so strong that it would not collapse after a large step strain. At a fixed entanglement density, e.g., using the same parent polymer at 10 wt % concentration, we show, by varying the extent to which the solutions are capable of undergoing interfacial wall slip, that the nonlinear relaxation behavior upon step shear is associated with macroscopic motions either in the bulk or at the sample/wall interface. The observed macroscopic motions are the result of sample recoil upon yielding of the strained entanglement network. It is the macroscopic recoil that accelerates the stress relaxation relative to that taking place quiescently at low strains. The different extent of motions occurring in the bulk and/or at the interface leads to relaxations ranging from type B to type C. As revealed using PTV, type B and A behaviors appear to be more closely related to internal bulk failure. On the other hand, solutions with great ability to undergo wall slip readily exhibit type C behavior.

It is only in reference to the DE theoretical prediction that the relaxation behavior has been traditionally grouped into type A, B, and C. This classification has no real meaning since none of these three types bear any relevance to the DE prediction. As explained elsewhere,[22,23] structural failure of a strained entanglement network is possible when the sufficiently high retraction force (due to the chain deformation during the step shear) overcomes the cohesive force arising from chain entanglement. The present work merely focused on visualizing what was responsible for the various relaxation behaviors from type A to C using particle-tracking velocimetry.

Acknowledgment. This work is supported, in part, by a Small Grant for Exploratory Research of the National Science Foundation (DMR-0603951) and an ACS grant (PRF #40596-AC7).

References and Notes

(1) Green, M. S.; Tobolsky, A. V. *J. Chem. Phys.* **1946**, *14*, 80.
(2) Doi, M.; Edwards, S. F. *The Theory of Polymer Dynamics*; Oxford University Press: Oxford, 1986.
(3) de Gennes, P. G. *J. Chem. Phys.* **1971**, *55*, 572.
(4) Einaga, Y.; Osaki, K.; Kurata, M.; Kimura, S.; Tamura, M. *Polym. J.* **1971**, *2*, 550.
(5) Einaga, Y.; Osaki, K.; Kurata, M.; Kimura, S.; Yamada. N.; Tamura, M. *Polym. J.* **1973**, *5*, 91.
(6) Fukuda, M.; Osaki, K.; Kurata, M. *J. Polym. Sci., Polym. Phys. Ed.* **1975**, *13*, 1563.
(7) Doi, M.; Edwards, S. F. *J. Chem. Soc., Faraday Trans. 2* **1978**, *74*, 1802, 1818.
(8) Doi, M. *J. Polym. Sci.* **1980**, *18*, 1005.

(9) Osaki, K.; Kurata, M. *Macromolecules* **1980**, *13*, 671.
(10) Osaki, K.; Nishizawa, K.; Kurata, M. *Macromolecules* **1982**, *15*, 1068.
(11) Morrison, F. A.; Larson, R. G. *J. Polym. Sci., Polym. Phys. Ed.* **1992**, *30*, 943.
(12) Archer, L. A.; Larson, R. G.; Chen, Y. L. *J. Rheol.* **1995**, *39*, 519.
(13) Larson, R. G.; Khan, S. A.; Raju, V. R. *J. Rheol.* **1988**, *32*, 145.
(14) Sanchez-Reyes, J.; Archer, L. A. *Macromolecules* **2002**, *35*, 5194.
(15) Islam, M. T.; Sanchez-Reyes, J.; Archer, L. A. *Rheol. Acta* **2003**, *42*, 191.
(16) Archer, L. A.; Sanchez-Reyes, J.; Juliani *Macromolecules* **2002**, *35*, 10216.
(17) Juliani; Archer, L. A. *J. Rheol.* **2001**, *45*, 691.
(18) Osaki, K. *Rheol. Acta* **1993**, *32*, 429.
(19) Venerus, D. C. *J. Rheol.* **2005**, *49*, 277.
(20) Vrentas, C. M.; Graessley, W. W. *J. Rheol.* **1982**, *26*, 359.
(21) Marrucci, G.; Grizzuti, N. *J. Rheol.* **1983**, *27*, 433.
(22) Wang, S. Q.; Ravindranath, S.; Boukany, P.; Olechnowicz, M.; Quirk, R.; Halasa, A.; Mays, J. *Phys. Rev. Lett.* **2006**, *97*, 187801.
(23) Wang, S. Q.; Ravindranath, S.; Wang, Y.; Boukany, P. *J. Chem. Phys.* **2007**, *127*, 064903.
(24) Wang, S. Q. *Adv. Polym. Sci.* **1999**, *38*, 227.
(25) Colby, R. H.; Rubinstein, M. *Macromolecules* **1990**, *23*, 2753.
(26) Colby, R. H.; Fetters, L. J.; Funk, W. G.; Graessley, W. W. *Macromolecules* **1991**, *24*, 3873.
(27) Yang, X.; Wang, S. Q. *Macromolecules* **1999**, *32*, 2638.
(28) Archer, L. A.; Larson, R. G.; Chen, Y. L. *J. Fluid Mech.* **1995**, *301*, 133.
(29) Vrentas, C. M.; Graessley, W. W. *J. Rheol.* **1982**, *26*, 359.
(30) Tapadia, P.; Wang, S. Q. *Phys. Rev. Lett.* **2006**, *96*, 019601.
(31) Boukany, P. E.; Wang, S. Q. *J. Rheol.* **2007**, *51*, 217.
(32) Brochard, F.; de Gennes, P. G. *Langmuir* **1992**, *8*, 3033.

MA071495G